Real-time release of Na, K and Ca during thermal conversion of biomass using quantitative microwave assisted laser-induced breakdown spectroscopy

J. Viljanen,[a] H. Zhao,[b] Z. Zhang,[b] J. Toivonen[a] and Z. T. Alwahabi[†,c]

[a] Laboratory of Photonics, Tampere University of Technology, FIN-33101, Tampere, Finland

[b] Key Laboratory of Thermal Science and Power Engineering of Ministry of Education, Department of Thermal Engineering, Tsinghua University, 100084 Beijing, China.

[c] School of Chemical Engineering, The University of Adelaide, S.A. 5005, Australia

[†] Email: zeyad.alwahabi@adelaide.edu.au

Abstract:

Power production with thermal conversion has met new challenges due the global pressure to use CO_2 neutral and renewable fuels, e.g. recycled fuel and biomass. Many of these fuels contain high concentrations of elements, such as alkali metals and chlorine, that together are harmful for boiler structures and may cause operational problems. Therefore, detailed quantitative information on release behaviour of the problematic elements, potassium and sodium, is required. For this, a new burner, which allows linear calibration of laser induced breakdown spectroscopy (LIBS) measurement toward higher concentrations relevant for the release studies during thermal conversion of biomass, was designed. The analytical performance of conventional LIBS measurement is significantly improved by introducing microwave radiation to the laser-induced plasma. An enhancement of linearity and up to 60-fold improvement of limit of detection (LOD) was observed with microwave-assisted LIBS (MW-LIBS) in comparison to conventional LIBS. The LOD of sodium (Na), potassium (K) and calcium (Ca) were 10 ppb, 19 ppb and 16 ppb, respectively. In-flame MW-LIBS measurement was applied to record time-traces of K, Na and Ca during thermal conversion of a poplar pellet. This is the first demonstration of Microwave near-field applicator injected MW-LIBS for gas phase measurement. With broad dynamic measurement range, the proposed method can be applied to extensive research of elemental release behaviour of different fuels. In addition to combustion studies, the MW-LIBS method can be extended to study trace-elements in gas phase in different fields of industry and science.

Keywords: *LIBS, combustion, microwave, flame, calibration*

1. Introduction

Concern of environmental aspects and the increasing price of fossil fuels are driving the power production towards renewable and CO_2 neutral energy sources. This has increased the interest on using low quality fuels, such as communal waste and biomass, for power production. However, these fuels are problematic for combustion boiler operation due to high release rate of alkali compounds.[1] KCl and NaCl have been found to cause severe slagging and fouling in the boiler structures that may lead to operational problems and unplanned shutdowns.[2] Detailed information on the release behaviour of the alkaline compounds is required and it has been under extensive research.

Multiple online methods are used to study the metal species in reactive flows and are extensively reviewed by Monkhouse.[2] Atomic absorption techniques, atomic absorption spectrometry (AAS)[4], differential optical absorption spectrometry (DOAS)[5], and their applications,[5,6,7] offer element or molecule specific information but are limited to their specific species present in gas phase. In many combustion applications, it would be in interest to measure the total concentration of an elemental specie. This can be achieved with atomic emission methods, such as excimer laser-induced fragmentation fluorescence (ELIF)[8] or laser-induced breakdown spectroscopy (LIBS)[9] that, however, have limited operational range due the difficulties in calibration for broad measurement range.

LIBS has become one of the leading online elemental analysis techniques. Its ability to provide multi-element analysis, requirement of minimal or even no sample preparation, applicability to solid, liquid, and gas phase, and stand-off capability are the clear advantages of LIBS[11] when compared to other elemental analysis techniques, such as inductively coupled plasma (ICP) analysis methods and X-ray fluorescence (XRF) technology.[12] In recent years, LIBS technique has been widely applied in field of combustion diagnostics. For instance, equivalence ratios in laminar premixed flame,[13,14] non-premixed flame,[14,15] and turbulent partially premixed flame[14,16] were all measured by LIBS. Besides the laboratory flames mentioned above, LIBS has also been utilized for equivalence ratio measurements in spark-ignited engines.[17,18] In addition of the equivalence ratio detection, LIBS was employed for *in situ* measurement of temperature in partially premixed flame.[19]

Measurement of alkali metals in high temperature gases has been under extensive study. Molina *et al.*[20] studied the effect of the ambient gas to the LIBS signal and found that significant attenuation of the alkali metal LIBS signal occurred, when the stoichiometry of the gas surrounding the spark changed from fuel lean to fuel rich. He *et al.*[21] have been studying the effect of O_2 and CO_2 to the temporal behaviour of alkali metal release from coal particles and Zhang *et al.*[22] have recorded the potassium release during combustion of pine wood using LIBS. The LIBS results have also been applied in modelling of the alkali release from biomass fuels.[23] However, in the reported studies the calibration ranges have been limited to concentration of approximately 10 ppm[10,21,22] and this has been hindering extensive alkali release measurements from biomass fuels with more abundant alkali concentrations. Therefore, in order to make the in-flame LIBS detection of alkali metals more accurate and reliable, new LIBS calibration methods, which are able to provide linear calibration curves covering the practical high alkali metal concentration ranges in flame, are urgently needed.

The calibration of laser induced plasma emission signal is associated on the curves of growth, i.e. calibration curves. The curves are expressed to describe the relation between the intensity of the emission and the analyte number density in the plasma.[11] Ideally the calibration curve shows linear relation between the wavelength-integrated emission line intensity and the analytic concentration, and indeed, this is the case in optically thin environment, i.e. when self-absorption is negligible. In optically thick conditions, the linear dependency of the emission on analyte number density is lost due to self-absorption. In the most extreme case the collected analyte emission line is deteriorated by self-reversal effect. Compromises in the analytical performance has to be done to overcome these problems causing the nonlinearities in the curve of growth. Self-absorption either forces to focus on low concentration conditions or leads to a choice of another analyte emission line that is less prone to self-absorption.[24] The lines that are less influenced by the self-absorption usually originate from higher energy levels and therefore the use of these lines for the detection compromises the limit of detection (LOD) in conventional LIBS measurements. Recent development on microwave-assisted LIBS (MW-LIBS) has shown that, in addition to improvement of LOD, microwave assistance is capable to reduce the self-reversal and self-absorption in the plasma plume.[25] This is highly beneficial when measuring high elemental concentration samples that are prone to self-absorption.

The calibration of LIBS signal is not alone affected by the elemental absorption properties but also the calibration sampling plays an important role. The complex nature of interaction between laser and sample and between plasma and sample leads to undesirable matrix-effects. These effects cause variations in plasma properties that are dependent on sample material properties and laser characteristics.[11] Therefore, the calibration sample properties have to match with the actual sample and this may be very difficult to achieve without extensive sample preparation, which would cut down one of the LIBS's advantages. The calibration sample arrangement is not as difficult in the case of gas phase, as it is in solid phase, as the measurement configuration parameters, e.g. lens-to-sample distance and the sample homogeneity, are easy to maintain. However, most elements, e.g. alkali metals and alkaline earth metals, are not commonly found in gas phase and therefore reliable calibration of metallic analytes to high concentration levels have found to be challenging. Controlled gas phase concentrations have been produced by evaporating salt compound containing the desired analyte letting the vapour pressure reach equilibrium.[26] Even though the equilibrium method can produce considerable concentration of the analyte into the gas phase, it requires very stable atmosphere to reach the equilibrium. Therefore, this method is rarely suitable for LIBS applications. The salt can be also seeded into the measurement volume as aerosol. Aerosol is produced with nebulizer and carried with gas flow into a heated measurement volume where the aerosol is vaporized.[10] However, in the seeding method demonstrated by Hsu *et al.*[10] the aerosol is carried to the flame by the combustion gas that limits the ability to vary the amount of aerosol injected into the flame. High concentration calibration would require high number of aerosol droplets injected into the flame. In the former design variation in the carrier gas flow would lead variation in the flame properties that would compromise the validity of the calibration. On the other hand, changing the analyte concentration in the nebulized solution affects to the efficiency of nebulization, hence, may lead to nonreliable calibration of the measurement.

This paper addresses the issues in quantitative LIBS calibration related to combustion studies by using novel approach for analyte seeding. This was achieved by introducing aerosol containing

the analye to centre of the flame only using novel burner design. The analytical performance was further improved introducing microwave-assistance to the laser induced plasma with a microwave near-field applicator (NFA)[27]. NFA injected MW-LIBS has previously been applied to solid[25] and liquid[28] phase measurements. This study is the first demonstration of NFA in gas phase measurement. MW-LIBS has the ability to reduce self-absorption in high concentration conditions and improve LOD.[25] LIBS and MW-LIBS performances are compared in terms of LOD and linearity of the calibration curves for K, Na, and Ca. The obtained calibration curves are applied to measure temporal release curves of K, Na, and Ca during thermal conversion of poplar pellet inside the flat flame to demonstrate the applicability of the method in a biomass combustion environment.

2. Experimental set-up

2.1 Calibration sample seeding and burner design

Figure 1. shows a Hencken style flat flame burner with a single seeding tube in the centre. The burner was designed to provide a well-controlled combustion environment and suitable quantitative seeding of alkali salt solutions to the flame. The flat flame burner consists of an inner brass tube and an outer brass tube with the inner diameter of 23.4 mm and 40.5 mm, respectively. The inner brass tube is divided into two parts and connected by a fringe in the bottom part. The burner can be divided into four main parts, namely fuel jets, air co-flow, N_2 shroud flow, and seeding flow. There are 58 stainless steel hypodermic tubes with the diameter of 1 mm, which are fixed evenly on a stainless-steel disk in the connecting fringe. CH_4 is fed through a packed bed into all the tubes to ensure a uniform fuel flow in each tube. These tubes convey CH_4 to the outlet of the burner and emerged as the fuel ports on the surface of the honeycomb. The combustion air flows into the inner brass tube via side tubes and is conveyed upstream through a packed bed and a stainless-steel honeycomb, forming the co-flow. Each fuel jet is directly adjacent to 6 hexagonal air co-flows to form the uniform flat flame. The shroud N_2 flow is fed into the outer brass tube via side tubes and through a packed bed and a stainless-steel honeycomb to stabilize the inner flat flame. The central tube with a diameter of 1 mm was used to seed the salt droplets into the flame in the LIBS calibration system.

The seeding was realized using salt solutions that were nebulized and carried into the flame. An ultrasonic nebulizer was employed to produce a fog of droplets from different salt compound (KCl, NaCl or $CaCl_2$) solutions in a sealed tank. A flow of pre-mixed CH_4 and air passing through the tank carried the nebulized droplets via the central hypodermic tube that was drilled through the bottom of the inner brass tube into the centre part of the flat flame. The droplets were vaporized by the heat when injected into the flame. By changing the flow rate of the carrier gas, the seeding rate of the droplets of the solutions into the flame could be precisely controlled. Thermal mass flow controllers (MFCs) from Bronkhorst High-Tech were used to determine the separate flows of CH_4, air and nitrogen.

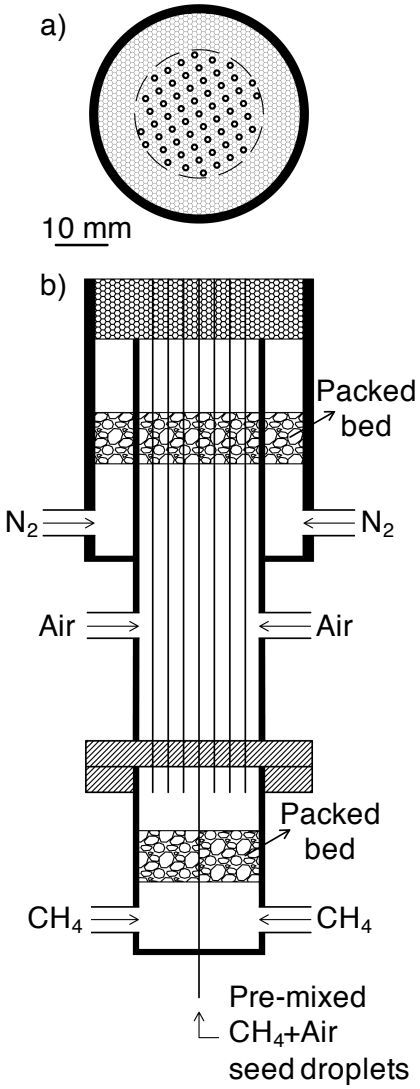

Figure 1 The sketch of the flat flame burner. a) Top view, b) cross-section view.

In order to make the flat flame working in the lean and temperature stable condition in the LIBS calibration experiment, the flow rate of the air and fuel CH_4 were set to be 5.0 L/min (STP) and 410.0 mL/min (STP), respectively. Therefore, the equivalent ratio was about 0.78. The equivalent ratio of the seeding flow was also set to be 0.78. The flow rate of the seeding flow was controlled in the range from 10 to 180 mL/min (STP) for this study.

A gravimetric approach was used to determine the mass flow of salts into the flame. The nebulizer tank was weighted before and after a seeding period of 12 hours on an analytical balance to evaluate the rate of mass loss. The concentrations of the NaCl, KCl and $CaCl_2$ solutions in the nebulizer tank were 100 g/L that was found to be close to the maximum to maintain nebulizer operation constant and to avoid blockage of pipes. It was observed that the droplet generation by the nebulizer was much faster than the seeding depletion up to flow rate of 110 mL/min after which the droplet density started to decrease in the reservoir tank. Thus, it is assumed that the number density and droplet size in the nebulizer tank did not change when

the seeding CH_4 flow rate changed in range of 10 to 100 mL/min. As a result, the liquid mass consumption rates between the seeding flow rate of 10 mL and 100 mL/min were calculated by interpolation, and the seeding rate of the alkali compound into the flat flame could be given

$$SR_a = A \cdot Q_{neb} \cdot SC \quad (1)$$

where SR_a is the seeding rate (g/min) of the alkali compound into the flat flame, A is the mass loss constant for the solution, Q_{neb} is the seeding flow rate (mL/min), and SC is the alkali compound solution concentration (g/mL) in the nebulizer tank.

2.2 MW-LIBS arrangement

A schematic presentation of the optical measurement arrangement is shown in Fig. 2. Laser induced plasma was achieved by focusing a frequency doubled Nd:YAG laser pulse with wavelength of 532 nm, 8 ns pulse width, 10 Hz repetition rate and 70 mJ pulse energy (Quantel YG) 22 mm above the burner surface. The laser pulse energy was tuned with a Glan laser polarizer and a half-wave plate to provide stable and repeatable plasma in the measurement conditions used in the study. With 70 mJ the laser induced plasma plume size was sufficiently small to avoid contact and, hence, contamination from the NFA. A plano-convex lens with 100 mm focal length was used to focus the laser in the centre of the flame. The plasma emission was collected with a perpendicular collection arrangement using two plano-convex lenses with 100 mm and 50 mm focal length to collect the plasma emission in to an optical fibre having 1 mm core diameter (Thorlabs). The emission was separated into a spectrum using Andor Shamrock monochromator (SR-500) equipped with 2400 g/mm and 1200 g/mm gratings. The spectral resolution of the spectrometer, with the 2400 lines/mm grating, is 0.031 nm at ~325nm, with a resolving power of 10,000. The spectra were recorded with Andor iStar ICCD camera.

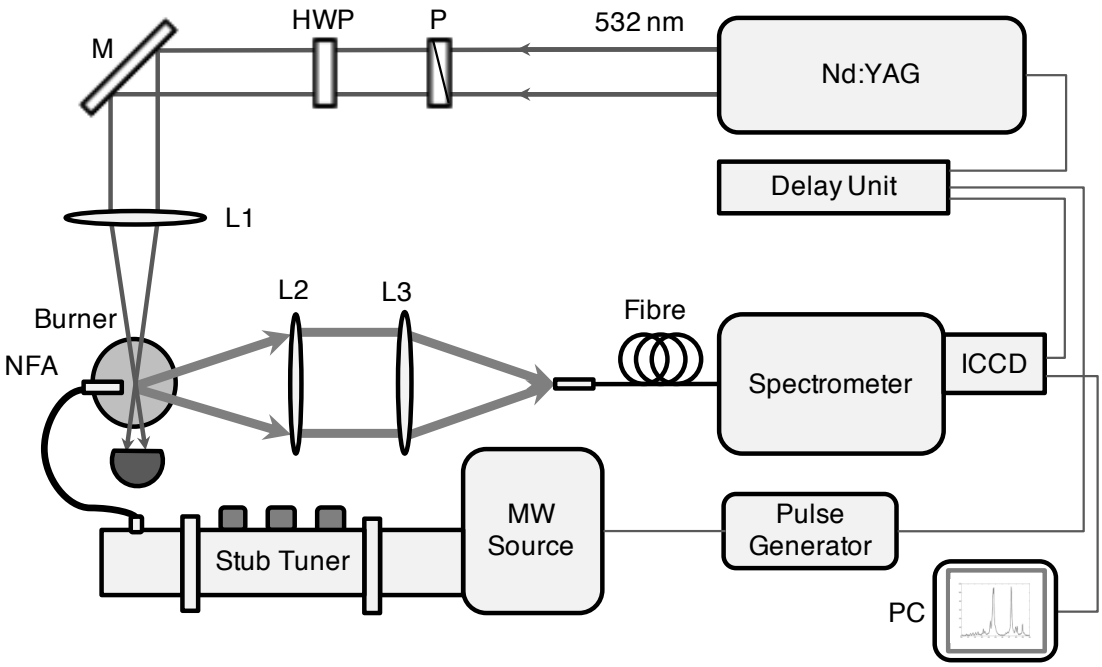

Figure 2. The experimental arrangement used for Na, K and Ca detection during biomass combustion: polarizer, P; half-wave plate HWP; mirror, M; lens, L; near-field applicator, NFA.

Pulsed microwave radiation with 1.5 ms pulse width and 600 W peak power was generated with Sairem microwave system. The radiation was coupled into a coaxial cable (50 Ω NN cable) with attenuation of 0.14 dB @ 2.45 GHz using a waveguide-to-coaxial adaptor. The maximum power level was chosen to be 600 W to avoid overheating in the adaptor when using microwave pulses with duration over 1 ms. This, however, was not limiting significantly the enhancement effect as the enhancement factor saturates when microwave power is increased[25,28]. Radiation was delivered to the laser induced plasma using specially designed NFA[27]. NFA was placed 0.5 mm away from the laser induced plasma in perpendicular orientation in respect to laser pulse propagation. The microwave pulse was launched 300 μs before laser pulse to ensure that microwave power reaches the maximum level when the initial plasma plume is ignited by the laser pulse. However, the microwave radiation is not absorbed to the plasma instantly after its ignition due the high electron density in the early state of the laser induced plasma. The initial plasma electron density was approximated to be 7×10^{18} cm^{-3} using the stark broadening of hydrogen emission line at 656.27 nm[29]. Microwave radiation can penetrate the plasma surface as the plasma electron density is sufficiently decayed. The electron density of microwave-maintained plasma was approximated to be 8×10^{15} cm^{-3}. More detailed description of the interaction between NFA injected microwave radiation and plasma is a topic of another research.

3. Results and discussions

3.1 Burner and seeding characteristics

The radial temperature profile of the flame in used biomass thermal conversion conditions is shown in Fig. 3. The temperature was measured with an R-type thermocouple and corrected for radiation. It is seen from Fig. 3 that the radial temperature profile of the flame is spatially uniform (<80 K) within the radius of 4 mm at the LIBS measurement height of 22 mm from the burner surface. At 22 mm above the surface burner, the flame has the maximum temperature of 1497 ± 60 K at the centre line.

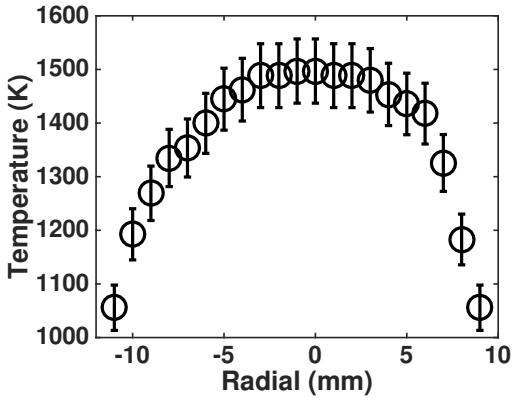

Figure 3. Radial flame temperature, at 22 mm above the burner surface, with equivalence ratio of 0.78.

The average concentration of the analyte species inside the flat flame could be calculated with knowledge of the alkali compounds seeding rate, as presented in Eq. 1, the flow rate of the fuel

and air, and the seeding flow rate. The horizontal average of analyte concentration (volume of the alkali elements per volume of the gas) is given by the following equation

$$C_a = \left(\frac{n \cdot SR_a}{MW_a}\right) / \left(\left(Q_{fuel} + Q_{air} + Q_{neb}\right) \cdot \frac{P}{RT}\right) \cdot 10^6 \quad (2)$$

where C_a is the average analyte concentration (ppm) on a horizontal plane of the flat flame at any height above the burner surface, n is the atomic number of the target atomic element in the compound, MW_a (g/mmol) is the molecular weight of the analyte compound, Q_{fuel} is the flow rate of the fuel CH_4, Q_{air} is the flow rate of the air, P is the atmospheric pressure, R is the universal gas constant, and T is the temperature in standard condition.

However, the distribution of analyte species in the flame is influenced by the seeding rate. To obtain the actual concentration of the seeded analyte in the measurement spot, the average value from Eq. 2 has to be corrected using a distribution function. The relative lateral distribution of the analyte concentration on the measurement height of 22 mm with different flow rates were measured using LIBS measurement. Sodium was used as a target analyte in this measurement and it was seeded as NaCl into the flame. The measured distributions are presented in Fig. 4. The measured emission intensities of sodium D1 line were fitted with Gaussian distribution function that was assumed due diffusion behaviour of molecular species. Using these distribution functions, the average analyte concentration in the flame obtained with Eq. 2 was corrected to correspond the concentration in the centre of the flame that was used as the measurement point.

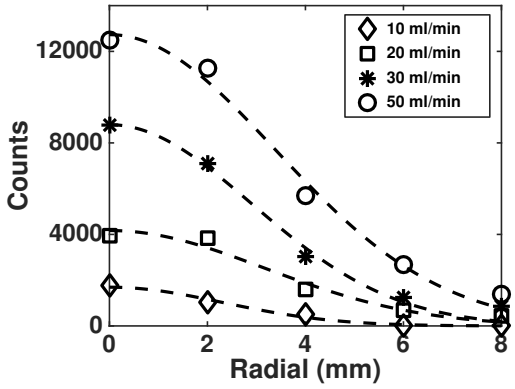

Figure 4. Concentration profile in the flame on different seeding flow rates. The measurement points are fitted with Gaussian curves that were assumed due diffusion behaviour of molecules

3.2 Spectral profile correction

The acquired LIBS emission line spectrum is affected by the absorption to the atomic population in the surrounding flame, in addition to the self-absorption familiar from previous LIBS studies[10], as Molina *et al.* have noted[20]. A theoretical correction is applied to the recorded spectrum to circumvent the nonlinear relation between the concentration and signal intensity caused by self-absorption, both in plasma and in the surrounding flame. The recorded spectrum S(ω) is a

product of two optical processes, namely, emission from the excited atoms H(ω) and absorption by the atoms at the ground state G(ω)

$$S(\omega) = H(\omega)G(\omega) = \frac{I}{1+\left(\frac{2(\omega-\omega_0)}{\gamma}\right)^2} exp\left(-\frac{\alpha L}{1+\left(\frac{2(\omega-\omega_0)}{\sigma}\right)^2}\right) \quad (3)$$

where *I* is the intensity at the emission maximum, γ and σ are the full width at half maximum of emission and absorption profile, respectively, and αL is the absorbance. The recorded spectrum was fitted with Eq. 3 using nonlinear least squares method using four independent variables, *I*, αL, γ and σ. Based on the best fit, the value of *I* is extracted to plot H(ω). An example of the fitting scheme is shown in Fig. 5. The extracted emission intensity profile is then integrated and compared against seeded analyte concentration in the flame to obtain the calibration data and further the desired release information.

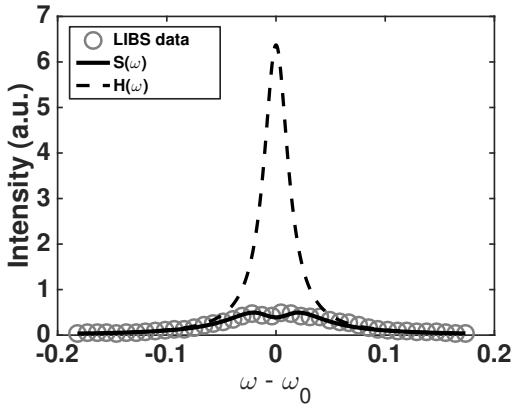

Figure 5. An example of absorption correction with the fitting method. S(ω) is the fitted line shape to the measured signal marked with circles and H(ω) is the emission profile extracted from the fitted function.

As shown in Fig. 6, the integrated H(ω), named self-absorption corrected MW-LIBS signal, has linear relation to the seeded Na concentration. In contrast, the integral of S(ω) suffers from the self-absorption and the linearity of the calibration is compromised leading to quadratic relation between seeded Na concentration and the signal counts in the calibration range. The extended linear range of the calibration curve compared to previous studies[10,21,22] improves the analytical sensitivity and reliability in high concentration environment and enables use of the method to measure alkali release behaviour from high alkali content fuels. It can also be noted that the relative standard deviation of the measured counts does not significantly increase due the spectral fitting procedure when standard deviations of 200 measured laser shots are compared.

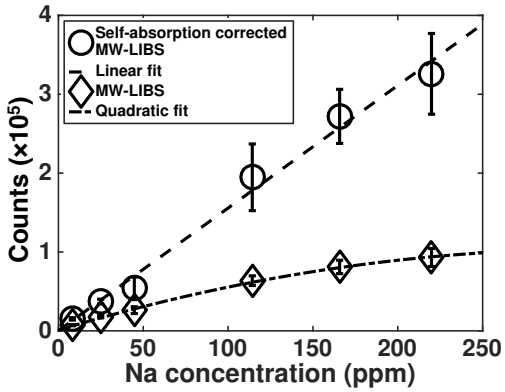

Figure 6. The effect of self-absorption correction to the calibration curve. Error bars represent the standard deviation of 200 measured laser shots.

3.3 MW-LIBS calibration

The calibration was conducted for Na, K, and Ca with both LIBS and MW-LIBS methods to compare their performance. For LIBS measurement, the optimal gate width and gate delay in terms of signal to noise ratio (SNR) were determined separately for each analyte element and are listed in Table 1. Measurement of K required much longer delay time to Na and Ca due interfering emission from other species present in the laser induced plasma that decayed in approximately 8 μs and enabled clearer distinction of K emission line. For MW-LIBS measurement the gate delay for each element was the same as in LIBS measurement and the gate width used for all was 1 ms. The ICCD camera gain for LIBS measurements was set on 100 whereas for MW-LIBS measurements the gain was set on 1 to avoid detector saturation in high concentration conditions. Examples of collected MW-LIBS and LIBS single shot K spectra are presented in Fig. 7. The data points used for calibration are averages of 200 laser shots.

Table 1 Elemental emission lines used in measurements and the optimized gating settings

Element	Wavelength (nm)	A_{ki}^{30} (10^7 s^{-1})	E_i^{30} (eV)	E_k^{30} (eV)	Gate delay (μs)	Gate width (μs)
Na	588.995	6.16	0.00	2.10	2.0	15.0
K	766.490	3.8	0.00	1.62	9.0	8.0
Ca	422.673	2.8	0.00	2.93	0.5	6.0

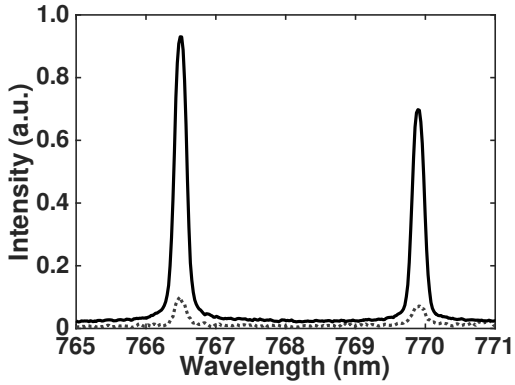

Figure 7. Typical single shot K D-line spectrum. Spectra acquired with MW-LIBS is presented with solid line and LIBS with dotted line.

The obtained calibration curves for Na, K and Ca are presented in Fig. 8. It was noted that the nebulizers ability to maintain the saturated condition in the sample reservoir was seed molecule dependent. It was visibly observed that with high injection flows the aerosol cloud inside the reservoir became less dense. Also, as the injection flow exceeded the threshold with which the nebulizer could not maintain saturated condition, the calibration curve showed a plateau and therefore calibration range varies between the elements. The measured points are fitted with linear curves. The slopes of the fitted curves are listed in Table 2. The calibration curves for MW-LIBS measurements are significantly steeper than those of LIBS measurements and possessed better linearity in terms of R^2 value. This indicates better sensitivity for MW-LIBS measurements. To compare the performances further, the LOD for LIBS and MW-LIBS were calculated using

$$LOD = ks_b/b \quad (4)$$

condition where k = 3, s_b is the standard deviation of the background and b is the slope of the calibration curve.[11] The computed LOD's are listed in Table 2. It shows that microwave assistance has the ability to extend the detection range in the low concentration cases with up to 60-fold improvement of LOD when compared to conventional LIBS. The achieved LOD's for Na and K are also improved over 3-fold when compared to the lowest LOD's reported in previous flame studies[10]. The LOD's are significantly lower than those reported for other elements in solid and liquid samples[25,28] due the high-temperature environment where the sample is already vaporized and the energy required to dissociate the alkali containing molecules is reduced. It is worth emphasizing that increasing the detector gain during MW-LIBS measurement would further lower the LOD, however, this would lead to detector saturation in high concentration case that was not desirable in the current application.

Table 2 Elemental calibration slopes and limits of detection achieved in this work and reported in previous flame studies.

	LIBS					MW-LIBS		
Element	Slope (counts / ppm)	R^2	LOD (ppb) This work	LOD (ppb) Previous work	Ref.	Slope (counts / ppm)	R^2	LOD (ppb) This work
Na	407.3	0.95	125	29	[10]	3108.8	0.98	10
K	490.8	0.91	408	72	[10]	6536.2	0.99	19
Ca	35.9	0.94	945			1668.6	0.99	16

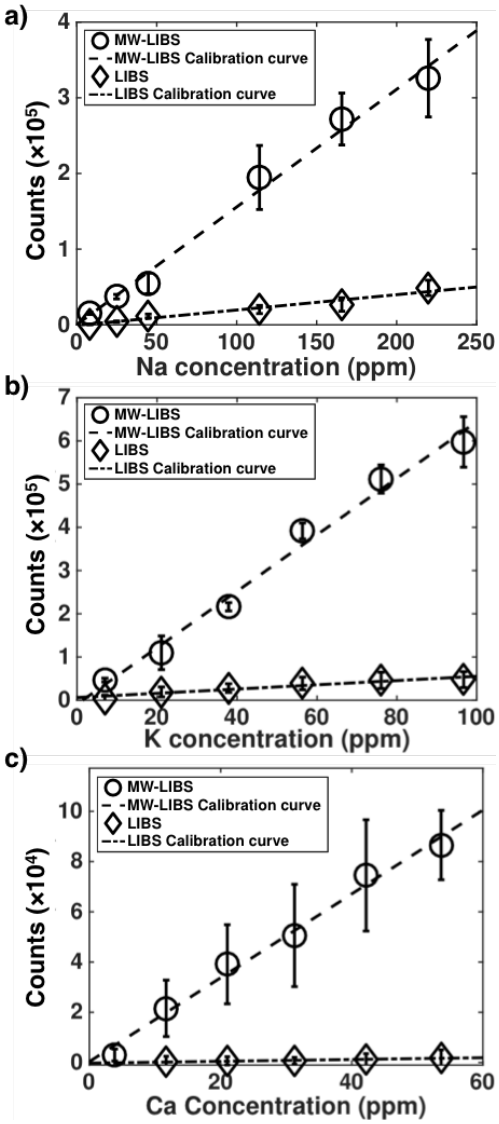

Figure 8. Calibration curves for a) Na, b) K and c) Ca. Error bars represent the standard deviation of 200 measured laser shots.

3.4 Temporal quantitative measurement of alkali release during thermal conversion of biomass

An application of the measurement technique is demonstrated measuring temporal total elemental release during thermal conversion of biomass samples. The samples were grained and pressed to pellets. Poplar was chosen as the sample to work with due to steady and repeatable behaviour during the conversion. The composition of ash-forming elements in the poplar was studied with chemical fractionation[31] and the results are presented in Table 3. The pellet with inset dimension of 2.5 mm in diameter was set to the centre of the burner 5 mm above the burner surface using platinum wire. The MW-LIBS measurement was conducted at a 14.5 mm distance from the particle surface. The measurement distance was over 5 times the particle dimeter from the particle surface so that the flame disturbance is minimal due the sample particle as observed previously[10,22]. To be able to use the line fitting method, MW-LIBS spectra were collected with relatively high spectral resolution. The maximum range was ~13 nm which

not enough to cover the selected lines of K, Na and Ca at 766.49 nm, 488.995 nm and 422.673 nm, respectively. It was necessary to record the release patterns of different species separately.

Table 3 Ash-forming elements in the poplar sample

Element	Cl	K	Na	Ca	Si	Al	Fe	Mg	Mn	P	S
Mass fraction (mg/kg)	702	2910	39.3	4150	102	31	61	445	4	858	196

The obtained time-traces of Na, K and Ca release are shown in Fig. 9. As expected, the more volatile Na, and K have much higher release rate than the Ca that is known to be mostly left into the bed ash[32]. A slight increase in Ca release rate is recorded during devolatilization phase while during char burning phase Ca MW-LIBS emission signal is hovering close to LOD. The release rate of K towards the end of char burning rises above the calibration range, hence these values cannot be considered reliable in terms of quantitative measures. However, the trend is clear that the relative K release is very high in the end of char burning. The release pattern of Na and K follows similar trend as in the previous measurements done for wooden samples[7,10,22]. During devolatilization Na and K are released mostly as alkali chlorides and, as the conversion proceeds, the char associated alkaline atoms are released increasingly as free atoms and hydroxides increasing the total release towards the end of the char burning phase[7,23]. K is showing significantly higher release during the conversion as expected based on the fuel analysis. The strong release during char burning is most likely due to the stoichiometric excess of K and Na to Cl that leaves most of the alkaline to the char after dechlorination during devolatilization.

The release patterns recorded during thermal conversion of poplar shows the potential and applicability of the proposed measurement method for combustion research. The calibration at high concentrations enables measurement targets to be extended to high volatile content fuels while application of MW-LIBS and its improved LODs allows the temporal measurement of trace elements. Hence, the broad dynamic range of the measurement enables more complete analysis of elemental release rates in combustion processes.

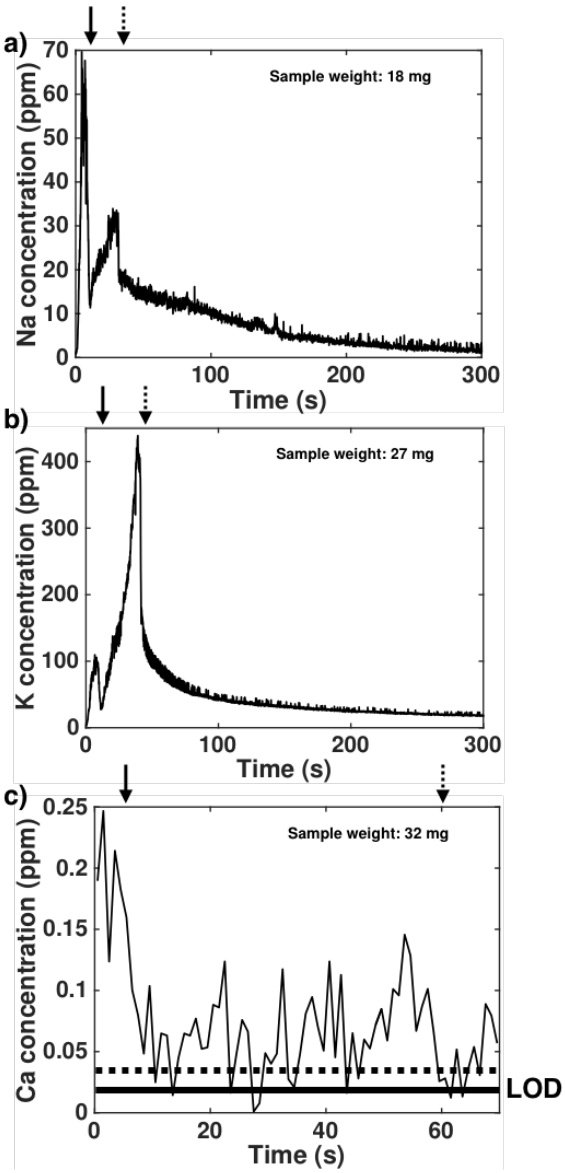

Figure 9. Temporal release of a) Na, b) K and c) Ca during thermal conversion of poplar with equivalence ratio of 0.79. Time-traces are measured using MW-LIBS and the spectral fitting method to extrapolate the calibration to high concentrations. The time trace of Ca release is averaged over 20 shots, i.e. 2 s, and cut to cover only the devolatilization and char burning to show the release during devoaltilization. The solid arrow marks the end of the devolatilization phase and the dashed arrow marks the end of char burning phase. Solid line in c) depicts the LOD for Ca measurement and the dashed line shows the measurement uncertainty at LOD.

4. Conclusions

Novel burner seeding method is presented to achieve broad LIBS calibration range for alkali measurement in combustion flame. The seeding method showed great potential for a linear from low to high concentration seeding limited only by the performance of the nebulizer used to create the seed reservoir. The performance and dynamic range is further improved by adding microwave assistance to the LIBS measurement being the first time when NFA injected MW-LIBS is demonstrated for gas phase measurements. The microwave assistance improved the LODs of the targe elements up to 60-fold. The LOD's for Na, K, and Ca were 10 ppb, 19 ppb and 16 ppb,

respectively. The trace element detection is demonstrated with Ca measurement during the biomass conversion. The calibration issues rising from self-absorption were diminished with computational correction that enabled linear calibration to high concentration conditions improving the method's analytical sensitivity and reliability for the alkali release measurements. The proposed method enables temporal alkali release measurements form wide range of biomass samples and therefore provides an important tool for combustion studies. The presented MW-LIBS method enables sensitive elemental analysis of gases also in different areas of industry and science.

Acknowledgements

This work has been partly carried out within CLIFF (2014-2017) as part of the activities of Tampere University of Technology. Other research partners are VTT Technical Research Centre of Finland Ltd, Lappeenranta University of Technology, Aalto University and Tampere University of Technology. Support from the National Technology Agency of Finland (Tekes), Andritz Oy, Valmet Technologies Oy, Amec Foster Wheeler Energia, UPM-Kymmene Oyj, Clyde Bergemann GmbH, International Paper Inc., and Top Analytica Oy Ab is gratefully acknowledged. Dr. Nikolai DeMartini is gratefully acknowledged for providing the samples. J. V. would also like to acknowledge the support by TUT Graduate school.

References:

1 H.P. Nielsen, F. J. Frandsen, K. Dam-Johansen and L.L. Baxter, The implications of chlorine-associated corrosion on the operation of biomass-fired boilers, *Prog. Energ. Combust.* 26 (2000) 283-298.

2 S. Enestam, D. Bankiewicz, J. Tuiremo, K. Mäkelä and M. Hupa, Are NaCl and KCl equally corrosive on superheater materials of steam boilers?, *Fuel* 104 (2013) 294-306.

3 P. Monkhouse, On-line spectroscopic and spectrometric methods for the determination of metal species in industrial processes, *Prog. Energ. Combust.* 37 (2011) 125-171.

4 N.H. Bings, A. Bogaerts and J.A. Broekaert, Atomic spectroscopy, *Anal. Chem.* 78 (2006) 3917-3946.

5 C. Forsberg, M. Broström, R. Backman, E. Edvardsson, S. Badiei, M. Berg and H. Kassman, Principle, calibration, and application of the in situ alkali chloride monitor, *Rev. Sci. Instrum.* 80 (2009) 023104.

6 Z. Qu, E. Steinvall, R. Ghorbani and F. Schmidt, Tunable diode laser atomic absorption spectroscopy for detection of potassium under optically thick conditions, *Anal. Chem.* 88 (2016) 3754-3760.

7 T. Sorvajärvi, N. DeMartini, J. Rossi and J. Toivonen, In situ measurement technique for simultaneous detection of K, KCl, and KOH vapors released during combustion of solid biomass fuel in a single particle reactor, *Appl. Spectrosc.* 68 (2014) 179-184.

8 T. Leffler, C. Brackmann, A. Ehn, B. Kaldvee, M. Aldén, M. Berg and J. Bood, Range-resolved detection of potassium chloride using picosecond differential absorption light detection and ranging, *Appl. Optics.* 54 (2015) 1058-1064.

9 M.P. Glazer, N.A. Khan, W. de Jong, H. Splithoff, H. Schürmann and P. Monkhouse, Alkali metals in circulating fluidized bed combustion of biomass and coal: measurements and chemical equilibrium analysis, *Energy Fuels* 19 (2005) 1889-1897.

10 L.-J. Hsu, Z.T. Alwahabi, G.J. Nathan, Y. Li, Z.S. Li and M. Aldén, Sodium and potassium released from burning particles of brown coal and pine wood in a laminar premixed methane flame using quantitative laser-induced breakdown spectroscopy, *Appl. Spectrosc*. 65 (2011) 684-691.

11 D.W. Hahn and N. Omenetto, Laser-induced breakdown spectroscopy (LIBS), part II: review of instrumental and methodological approaches to material analysis and applications to different fields, *Appl. Spectrosc.* 66 (2012) 347-419.

12 Y. Zhang, X. L. Zhang, W. B. Jia, Q. Shan, Y. S. Ling, D. Q. Hei and C. Da, Online X-ray fluorescence (XRF) analysis of heavy metals in pulverized coal on a conveyor belt, *Appl. Spectrosc*. 70 (2016) 272–278.

13 A. Michalakou, P. Stavropoulos and S. Couris, Laser-induced breakdown spectroscopy in reactive flows of hydrocarbon-air mixtures, *Appl. Phys. Lett.* 92 (2008) 081501.

14 J. Kiefer, J. W. Tröger, Z. S. Li and M. Aldén, Laser-induced plasma in methane and dimethyl ether for flame ignition and combustion diagnostics, *Appl. Phys. B-Lasers O* 103 (2011) 229-236.

15 A. E. Majd, A. S. Arabanian, R. Massudi and M. Nazeri, Spatially Resolved Laser-Induced Breakdown Spectroscopy in Methane—Air Diffusion Flames, *Appl. Spectrosc*. 65 (2011) 36-42.

16 M. S. Mansour, H. Imam, K. A. Elsayed and W. Abbass, Local equivalence ratio measurements in turbulent partially premixed flames using laser-induced breakdown spectroscopy, *Spectrochim. Acta. Part B.* 64 (2009) 1079-1084.

17 F. Ferioli, P. V. Puzinauskas and S. G. Buckley, Laser-induced breakdown spectroscopy for on-line engine equivalence ratio measurements, *Appl. Spectrosc.* 57 (2003) 1183-1189.

18 F. Ferioli, S. G. Buckley and P. V. Puzinauskas, Real-time measurement of equivalence ratio using laser-induced breakdown spectroscopy, *Int. J. Engine Res.* 7 (2006) 447-457.

19 T.-W. Lee and N. Hegde, Laser-induced breakdown spectroscopy for in situ diagnostics of combustion parameters including temperature, *Combust. Flame* 142 (2005) 314-316.

20 A. Molina, P. Walsh, C. Shaddix, S. Sickafoose and L. Blevins, Laser-induced breakdown spectroscopy of alkali metals in high-temperature gas, *Appl. Optics.* 45 (2006) 4411-4423.

21 Y. He, J. Zhu, B. Li, Z. Wang, Z. Li, M. Aldén and G. Cen, In-situ measurement of sodium and potassium release during oxy-fuel combustion of lignite using laser-induced breakdown spectroscopy: effects of O2 and CO2 concentration, *Energy Fuels* 27 (2013) 1123-1130.

22 Z. Zhang, Q. Song, Z. T. Alwahabi, Q. Yao and G. J. Nathan, Temporal release of potassium from pinewood particles during combustion, *Combust. Flame* 162 (2015) 496-505.

23 H. Fatehi, Y. He, Z. Wang, Z. S. Li, X. S. Bai, M. Aldén and K. F. Cen, LIBS measurements and numerical studies of potassium release during biomass gasification, *P. Combust. Inst.* 35 (2015) 2389-2396.

24 B. Le Drogoff, J. Margot, M. Chaker, M. Sabsabi, O. Barthe´lemy, T. W. Johnson, S. Laville, F. Vidal, and Y. von Kaenel, Temporal characterization of femtosecond laser pulses induced plasma for spectrochemical analysis of aluminum alloys, *Spectrochim. Acta. Part B* 56 (2001) 987-1002.

25 J. Viljanen, Z. Sun and Z. T. Alwahabi, Microwave assisted laser-induced breakdown spectroscopy at ambient conditions, *Spectrochim. Acta. Part B* 118 (2016) 29-36.

26 T. Sorvajärvi and J. Toivonen, Principles and calibration of collinear photofragmentation and atomic absorption spectroscopy, *Appl. Phys. B* 115 (2014) 533-539.

27 S. J. Chen, A. Iqbal, M. Wall, C. Fumeaux and Z. T. Alwahabi, Design and application of near-field applicators for efficient microwave-assisted laser-induced breakdown spectroscopy, *J. Anal. Atom. Spectrom.* 32 (2017) 1508-1518.

28 M. Wall, Z. Sun and Z. T. Alwahabi, Quantitative detection of metallic traces in water-based liquids by microwave-assisted laser-induced breakdown spectroscopy, *Opt. Express* 24 (2016) 1507-1517.

29 M. A. Gigosos, M. Á. Gonzáles and V. Cardeñoso, Computer simulated Balmer-alpha,-beta and-gamma Stark line profiles for non-equilibrium plasmas diagnostics, *Spectrochim. Acta. Part B.* 58 (2003) 1489-1504.

30 A. Kramida, Y. Ralchenko, J. Reader and NIST ASD Team (2018). NIST Atomic Spectra Database (ver. 5.5.6), [Online]. Available: https://physics.nist.gov/asd [2018, April 23]. National Institute of Standards and Technology, Gaithersburg, MD.

31 A. Pettersson, M. Zevenhoven, B. M. Steenari and L. E. Åmand, Application of chemical fractionation methods for characterisation of biofuels, waste derived fuels and CFB co-combustion fly ashes, *Fuel* 87 (2008) 3183-3193.

32 S. V. Vassilev, D. Baxter, L. K. Andersen and C. G. Vassileva, An overview of the composition and application of biomass ash. Part 1. Phase–mineral and chemical composition and classification, *Fuel* 105 (2013) 40-76.